Vortex interaction and breakdown over double-delta wings

S. L. Gai, M. Roberts, A. Barker, C. Kleczaj and A. J. Riley
School of Aerospace & Mechanical Engineering
University of New South Wales
Canberra, Australia

ABSTRACT

Modern high-speed aircraft, especially military, are very often equipped with single or compound delta wings. When such aircraft operate at high angles-of-attack, the major portion of the lift is sustained by streamwise vortices generated at the leading edges of the wing. This vortex-dominated flow field can breakdown, leading not only to loss of lift but also to adverse interactions with other airframe components such as the fin or horizontal tail. The wind tunnel and water studies described herein attempt to clarify the fluid mechanics of interaction between the strake and wing vortices of a generic 76°/40° double-delta wing leading to vortex breakdown. Some studies of passive control using fences at the apex and kink region are also described. Various diagnostic methods-laser sheet flow visualisation, fluorescent dyes, and pressure sensitive paints have been used.

1.0 INTRODUCTION

Typically, present day military aircraft operate at high angles-of-attack, usually 30° or higher. During manoeuvres the vortex-dominated flow over the wing can break down, leading to a loss of lift and also to adverse structural interactions, design of future military aircraft and also high speed civil transports. The fundamental fluid mechanisms behind the 'vortex breakdown' and 'vortex-vortex interactions' have yet to be clarified.

In the present investigation, we focus on the flow field over a 76/40° double-delta wing. This configuration is chosen since it is a good generic representation of modern military aircraft wing plan forms and also has been subjected to previous experimental and numerical studies[1-3].

The double-delta wing, at moderate to high angles-of-attack, exhibits a complex vortical flow field over the leeward side of the wing. Streamwise vortices form over the strake or forward and main wing sections, significantly increasing the lift and manoeuvrability of the wing. Experimental investigations in both water and wind tunnels over delta wings have in the past been thought to closely model the development of the flow field under full-scale flight conditions. However, more recent detailed investigations have found some inconsistencies, in terms of interaction and merging of the strake and wing vortices, between low and high/flight Reynolds number testing[2-4]. The fundamental mechanisms underlying these interactions and development of vortical structures are not very well understood and yet these are of prime importance if an aircraft is to operate at optimum manoeuvrability and safety.

Apex and inboard fences have been shown to have beneficial effects on swept wing flow fields, such as the delay in vortex breakdown, an increase in lift and stabilising of the nose-up pitching moment[5-7]. However, little detailed work has been done on the effect of fences on double-delta wings where the effect of fences on strake and wing vortices and their subsequent mutual interaction can be significant for the whole flow field on the wing. The optimisation and control of vortical flow fields over wings of fighter aircraft is today's most significant aerodynamic challenge. Addition of fences to the wing complicates what is already a complex and little understood flow field. To take full advantage of fences, which are passive, cheap and easy to maintain, it is important to fully understand their role in the vortex interaction mechanisms that occur over the wing. The present paper discusses some of these issues.

Paper No. 2770 . Manuscript received 15 July 2002, revised version received 7 May 2003, accepted 2 September 2003.

https://doi.org/10.1017/S0001924000004966 Published online by Cambridge University Press

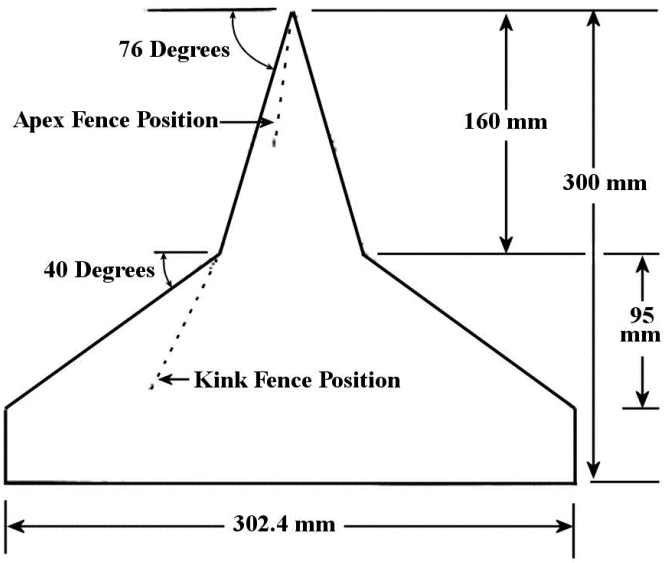


Figure 1. Planform and fence positions.

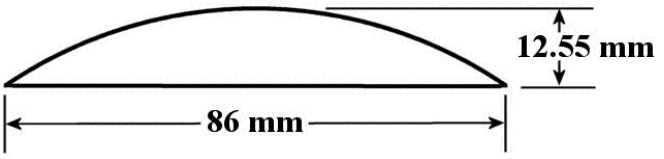


Figure 2. Fence shape.

2.0 EQUIPMENT

2.1 Tunnels

The wind tunnel experiments were conducted in a low turbulence wind tunnel whose test section was of cross-section 451mm × 451mm and length 2,130mm. The speed range of the tunnel was 0-45ms^{-1} and the turbulence level was less than 0·2%. The test section had a rectangular cut-out of dimensions 288mm × 105mm above the forward part to enable observation and recording from above.

Water tunnel experiments were conducted in a water tunnel, which had a test section of cross-section 304mm × 155mm and length 1,032mm. The maximum speed that could be achieved was 10cm/s. The uniformity of the flow was checked by the motion of the dye filament introduced into the flow at the entry to the test section and following its motion through the test section length.

2.2 Models

Two sets of models were used in the course of the experimental work during this investigation, one for the wind tunnel and a half-sized version for the water tunnel. The models were both 76/40° double-delta planforms as shown in Fig. 1.

The root chords were 300mm and 150mm for the wind and water tunnel models respectively. Both models had flat tops and sharp, 45° bevelled leading edges. The model plate thickness to chord (root) ratio was 0·03. The wind-tunnel model was made up of a base and two tops, one for flow visualisation and one fitted with 57 pressure tappings to measure pressure distributions. The flow visualisation top was painted black and scribed with lines at 10% graduations of chord from apex for laser sheet and smoke visualisations. It was subsequently cleaned and painted with pressure sensitive paint for the pressure sensitive paint testing. The pressure-tapped model had 9 pressure taps at 0·2 chord, 10 at 0·4, 1·5 at 0·6 and 23 at 0·8. The wind tunnel model was attached to a sting, which had a mount that allowed adjustment of the angle-of-attack from outside the tunnel. The mount also featured an angle-of-attack indicator and a fine yaw adjustment screws to align the model with the flow.

The water tunnel model was equipped with five ports in the surface for dye injection into the flow, with one just before and one just after the kink, and one at the model apex. The water-tunnel model was mounted on a sting attached to a cross-member running across the test section. This was attached through the side windows to a handle by which the angle-of-attack could be adjusted. Dye was injected into the model via lines running from dye reservoirs installed above the tunnel. The flow rate of the dye could be adjusted via a number of valves.

2.3 Fences

The fences used in this investigation were of the large double gothic type. They were designed based on research by Hoffler *et al*[5], which showed that fence effectiveness on delta wings is related primarily to the fence size relative to the model size, and that the double Gothic shape is more effective than other more simpler shapes. This agrees with the findings by Lamar[6], which showed that the most effective shape for the strake portion of the double delta is the Gothic shape. Hence the double gothic shape was chosen for the fences used in the present investigation. In order to keep fence size reasonable, the fence area was 7·5% of the model area, the length equal to 86mm and the height 12·55mm (Fig. 2). The thickness of the plates was 2·5mm.

The fences were positioned inboard of the leading edge in accordance with the findings by Wahls *et al*[7], which showed that this position is more effective on delta planforms for apex fences than along the leading edge. The fences were positioned approximately along the axis of vortices (as shown by the flow visualisation studies). This meant that the kink fences were approximately 26° inboard of the leading edge of the wing at the kink and the apex fences about 7° inboard of the leading edge at the apex. The fence positions are shown in Fig. 1.

3.0 EXPERIMENTAL TECHNIQUES

3.1 Wind-tunnel flow visualisation

The flow visualisation in the wind tunnel consisted of injecting the smoke ahead of the model through a thin probe and illuminating the model with white light allowing the full flow field to be observed. The images were then recorded on a digital video camera and stored in a computer.

Laser sheet smoke visualisation was also used. A 1·5mW helium-neon laser was used to project a sheet of light through a slot in the ceiling of the test section on to the model, illuminating a cross-section of the smoke injected into the flow using the probe as described above. The laser sheet was traversed to different chordwise positions in order to observe the development of the vortices along the model. Although it was not possible to capture images covering the full span of the model due to the narrow width of the slot in the test section ceiling, it was still possible to achieve coverage of the area of vortex interaction in all cases. Photographs were taken with a Sony Digital Handycam DCR-VX1000E digital video camera. The images were then stored in a computer. The use of a laser to illuminate a cross-section of the flow allows a higher flow speed to be used as it illuminates the smoke more strongly than the white light used in the full-field smoke visualisation. It therefore allows the interactions between the vortices to be better investigated as both vortex cores can be clearly visualised.

https://doi.org/10.1017/S0001924000004966 Published online by Cambridge University Press

3.2 Water tunnel flow visualisation

Visualisation was accomplished by injection of dye into the flow from five ports on the model as previously described. Control of dye injection was critical in this flow visualisation as excessive pressure meant too much dye was entrained in the vortex flow making observations difficult. Images were recorded using a Panasonic NV-DX100 digital video camera. They were then captured using Apple iMovie software. Fluorescent green dye was used to provide maximum visibility against black background. The flow was illuminated using white light and both side and top views of the flow were taken. The top view especially allowed the paths of the water-tunnel vortex interaction images to be compared to the wind tunnel ones.

3.3 Pressure sensitive paint

The PSP technique is heavily dependent on the use of digital imaging and processing. Fortunately there are commercially available softwares that can be implemented. The paint used in the present investigation was Innovative Science Solutions (ISSI) Unicoat Pt (TfPP)-FIB-Based PSP. The paint was excited using an ISSI LM@ LED pod, producing light in a narrow spectrum centred around 465nm. A Marumi R2 red filter was used on the camera to screen out light sources other than the paint. During the PSP measurements the wind tunnel speed was kept at 30ms^{-1}.

3.4 Discrete pressure tap measurements.

Discrete pressure tap measurements were made on the model in the wind tunnel using a Scanivalve system SSS 48C in conjunction with an MK 4 pressure transducer. This was connected to an interface unit and controlled via the scanivalve controller program running on a NEC Powermate 386 computer.

Prior to testing, the scanivalve pressure transducer was calibrated using a Druck DPI 610 pressure calibrator accurate to ±1 Pa. Overall, the pressure measurement system accuracy was of the order of ±1%.

These discrete pressure measurements were also made at a flow speed of 30ms^{-1} in order to directly compare with the PSP data.

4.0 FLOW CONDITIONS

In the case of the wind-tunnel, runs were made at different speeds depending on the flow visualisation technique used. Thus, for full flow smoke visualisation, the flow speed was kept quite low at 2·5ms^{-1} giving a Reynolds number based on root chord of $4{\cdot}7 \times 10^4$. For the laser sheet flow visualisation, the speed was 7ms^{-1} corresponding to a Reynolds number of $1{\cdot}3 \times 10^5$. During the acquisition of the pressure data, the tunnel was run at a speed of 30ms^{-1} and a Reynolds number of $5{\cdot}6 \times 10^5$

The water tunnel tests were conducted at a speed of 2·4cm/s giving a Reynolds number of $3{\cdot}6 \times 10^3$.

5.0 FLOW VISUALISATION RESULTS

5.1 Plain wing

With the plain wing, the first development of the strake vortex is noted at 5° angle-of-attack and by 10° both the strake and wing vortices are well developed but no interaction is evident nor the breakdown. By 20°, the strake vortex curves sharply outboard well downstream of the kink and the vortex breakdown occurs at approximately 0·85 chord as a result of interaction between the strake vortex and the wing vortex (Fig. 3).

The movement outboard of the strake vortex as it progresses downstream is due to the wing vortex pulling the strake vortex

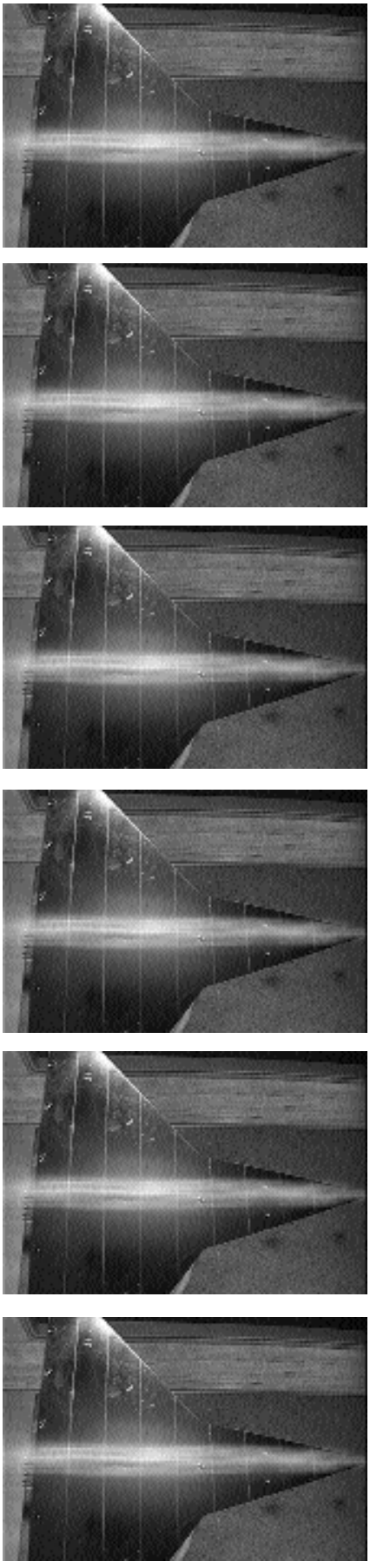


Figure 3. Full-field smoke flow visualisation over a plain wing (Re = $4{\cdot}7 \times 10^4$).

https://doi.org/10.1017/S0001924000004966 Published online by Cambridge University Press

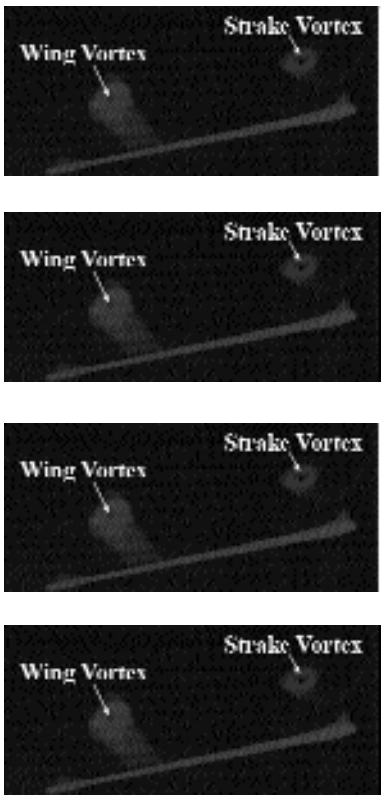


Figure 4. Laser sheet Images of vortex interaction ($\alpha = 20°$, $Re = 1{\cdot}3 \times 10^5$).

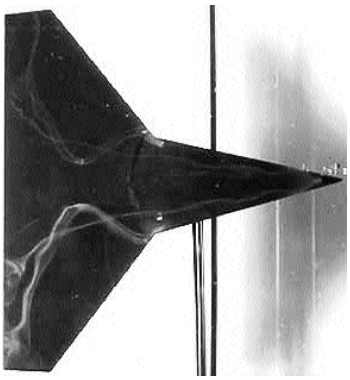


Figure 5. Full-field Water Tunnel visualisation over a plain wing ($\alpha = 25°$, $Re = 3{\cdot}6 \times 10^3$).

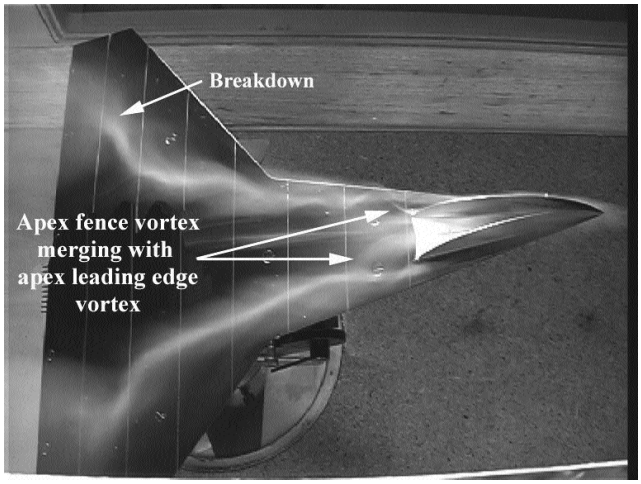


Figure 6. Strake vortex instability and breakdown over model with apex fences ($\alpha = 20°$).

outboard and down. Merging is facilitated by the wing vortex gradually enveloping the strake vortex. It does this by drawing fluid from the underside of the strake vortex core, growing, and finally enveloping the diminished strake vortex core. The process is clearly seen in Fig. 4. This type of interaction between the wing vortex and the strake vortex is termed the 'enveloping' type interaction. In this and subsequent figures (Figs 7-10) only one-half (the left side) of the wing is illustrated. The wing root is at the right hand edge of the photograph, while the tip is at the left hand edge. A different type of interaction can some times occur depending on the angle-of-attack and Reynolds number. Figure 5 shows a water tunnel dye flow visualisation of the model at 25° angle-of-attack. Here the strake vortex dominates the flow and it is seen to draw the wing vortex inboard and interaction takes place through the expanded wing vortex spiralling above and around the strake vortex core. The angular distortion of the vortex paths as a result of such interaction reaches a maximum at around 0·8 chord. When the breakdown eventually occurs, the strake vortex appears to breakdown first slightly ahead, chordwise, of the wing vortex. This is clearly seen in Fig. 5. This type of interaction is known as 'spiralling/coiling' interaction.

5.2 Apex fences

As in the case of the plain wing, vortices start to appear at 5° angle-of-attack and by 10°, the strake vortex is quite visible and strong but the wing vortex is not. At this angle-of-attack, there does not appear to be a clear breakdown, but rather, a gentle spreading of the core. The strake cores are less coherent than on the plain wing and are unsteady prior to the kink position. The outboard movement of the strake vortex occurs at approximately 0·68 chord (just aft of kink), moving the core approximately 15° from the original vortex path.

At 20°, the outboard movement of the strake vortex is still apparent aft of the kink, and breakdown position has advanced upstream to 0·8 chord. This is seen in Fig. 6.

Figure 7 shows the laser sheet visualisation at this angle-of-attack where the beginning of the spiralling interaction between the strake and wing vortex is seen. At 0·65 chord, the strake vortex is seen completely detached from the surface. However, instead of being stretched and drawn underneath the wing vortex core, the strake vortex core is quite circular and it appears that the wing vortex core is being drawn up and around the strake vortex. The process seems to be almost completed by 0·7 chord.

By 30°, angle-of-attack, the strake vortex breakdown has moved upstream, fluctuating between approximately 0·65 and 0·7 chord. The flow was quite unsteady and there was no strong outboard movement of the vortex prior to breakdown, in line with the plain wing results. The coiling interaction was again evident. Laser sheet visualisations showed that the strake vortex lifted off the surface and appeared to draw the wing vortex upwards and inboard but did not draw the wing vortex core over itself to the same extent as at lower angles-of-attack.

5.3 Kink fences

No vortex was visible until 5° angle-of-attack and at 5°, the strake vortex is drawn outboard and into the kink fence vortex on the inboard side. This continued up to 10° and is depicted in Fig. 8.

As seen in Fig. 9 at 15° angle-of-attack, the strake vortex deviates outboard and upwards, beginning 0·6 chord and continuing until 0·8 chord, where it appears in contact with the fence. It moves back inboard and downwards post-fence, as well as appearing less coherent. We can also see secondary vortices outboard of the strake vortex. There is no evidence of definite breakdown. The laser sheet visualisation of Fig. 9 also shows the merging of the strake vortex and the kink fence vortex inboard of the fence at 0·65 chord. The kink fence vortex appears to be lifted off the surface and is not fully developed. A coiling interaction appears to be developing between the kink fence vortex and strake vortex in which the cores eventually

https://doi.org/10.1017/S0001924000004966 Published online by Cambridge University Press

merge into a single vortex. Expansion of the combined vortex appeared to occur at approximately 0·85 chord but a stable and coherent vortex was still seen beyond this with some evidence of breakdown.

A similar pattern was observed at 20° but the deviation of the strake vortex was substantially reduced. The inboard motion post-fence was still there. The vortex does not breakdown as on the plain wing, but seems to become somewhat diffused at approximately 0·95 chord.

The laser sheet visualisation in Fig. 10 shows that while at 0·7 chord the kink fence and strake vortex cores are separate and distinct, the kink fence vortex core becomes elongated upon moving over and inboard of the strake vortex core at 0·8 chord. The vortex cores merge and a stable vortex is seen even at 0·9 chord. At 30° angle-of-attack, the vortex breakdown occurred at 0·6 chord and no deviation of the core prior to breakdown was discernible. Also, the vortex breakdown was noticeably less severe than for the plain wing.

6.0 PRESSURE MEASUREMENTS

Both discrete pressure tap measurements and pressure sensitive paint measurements were conducted at various angles-of-attack for the plain wing and wing with fences. The pressure tap data were corrected for tunnel blockage effects. The plain wing data was similar to the previous data obtained in this tunnel as well as the data obtained by Verhaagen[1].

Figure 11 shows a typical example of results obtained with pressure sensitive paint. The dark blue pixels indicate the strake vortex and the pink region in the junction region shows the wing vortex. At this angle, interaction between the strake vortex and the wing vortex can be seen as a region of high suction between the two vortices.

With increasing angle-of-attack, the interaction becomes stronger and vortex breakdown is seen at 22·5° angle-of-attack, as shown in Fig. 12. At 30° angle-of-attack, there is complete loss of suction as the vortex breakdown position has moved near the kink (Fig. 13).

A comparison of pressure tap results with the PSP data showed, in general, reasonable agreement. In terms of C_P values, the differences were small (of the order of 10%) at lower angles-of-attack but were as large as 30% at angles greater than 20°. Such a variation has also been noted by Klein[9] who found differences of the order of 41% between pressure tap and PSP data on a double-delta wing at an angle-of-attack of 22°. He comments that with increase in angle-of-attack, the intensity of light tends to become 'noisier' as a result of changes in distances from the surface to the light source as well as the angle of the surface to the incident light rays.

Figures 14(a, b and c) show the pressure plot data for the plain wing and wing with fences at an angle-of-attack of 20° at chordwise stations, 0.2, 0·4, 0·6, and 0·8 chord respectively. The curves indicate discrete pressure tap data in terms of C_P and the relevant position to each set of results is indicated by the horizontal lines below the curves. The figure is qualitative and not to scale but indicates, in general terms, the strake and wing vortex strength, their relative magnitude, and vortex breakdown as well as interaction intensity. A small inboard movement of the strake vortex due to interaction with the kink fence vortex is also evident.

7.0 CORRELATION OF PRESSURE DATA IN TERMS OF VORTEX HALF-WIDTH

Greenwell and Wood[8] proposed a method of quantifying the vortex breakdown on a delta wing using the pressure distribution data. A characteristic change in the vortex half-width was used as an indication of vortex breakdown. Greenwell and Wood further found that this technique for identifying the breakdown could either be used when vortex half-width was plotted against angle-of-attack, or when plotted against chordwise position.

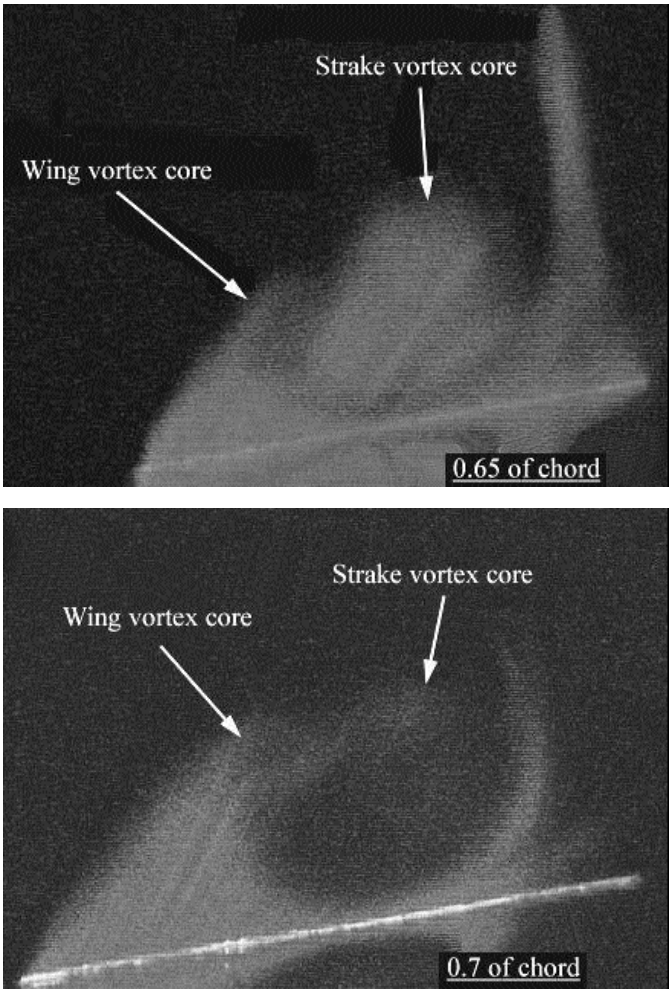


Figure 7. Beginning of spiralling interaction, model with apex fences ($\alpha = 20°$, $Re = 1{\cdot}3 \times 10^5$).

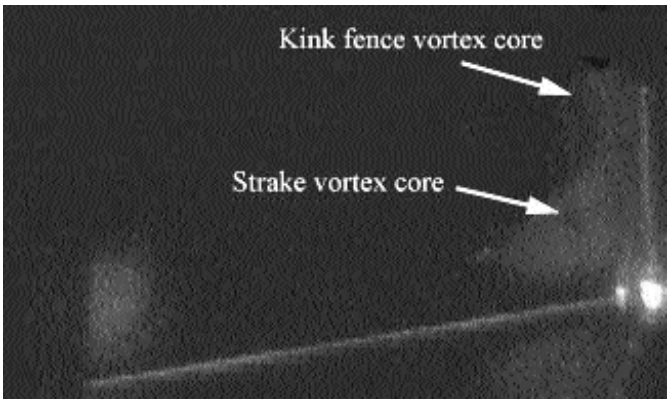


Figure 8. Initial vortex interaction at kink fence, 0·65 chord. ($\alpha = 10°$).

https://doi.org/10.1017/S0001924000004966 Published online by Cambridge University Press

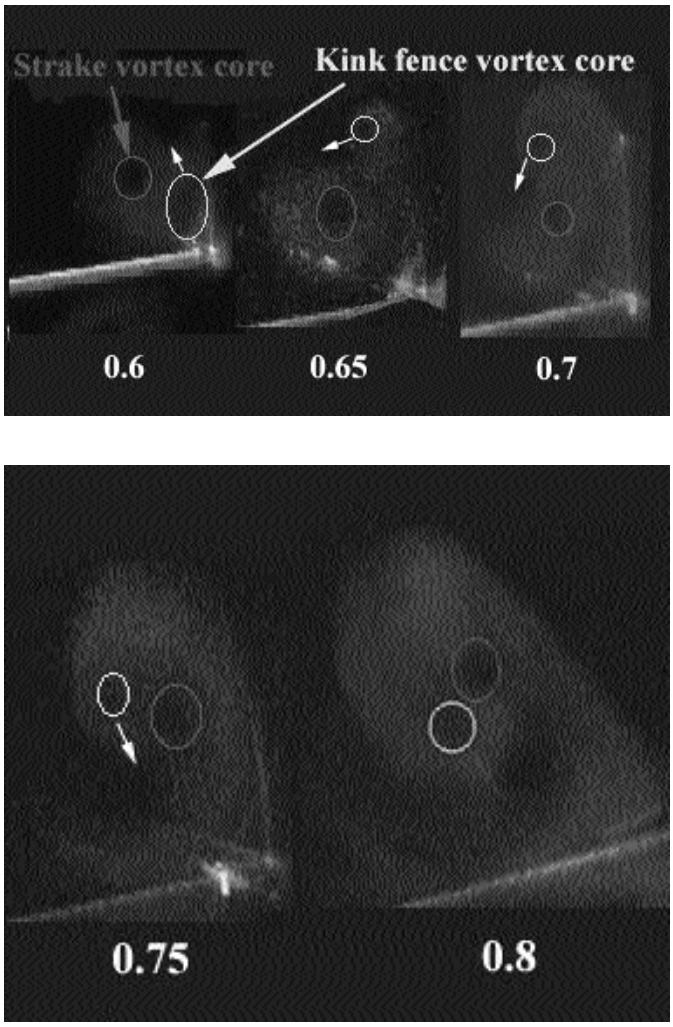
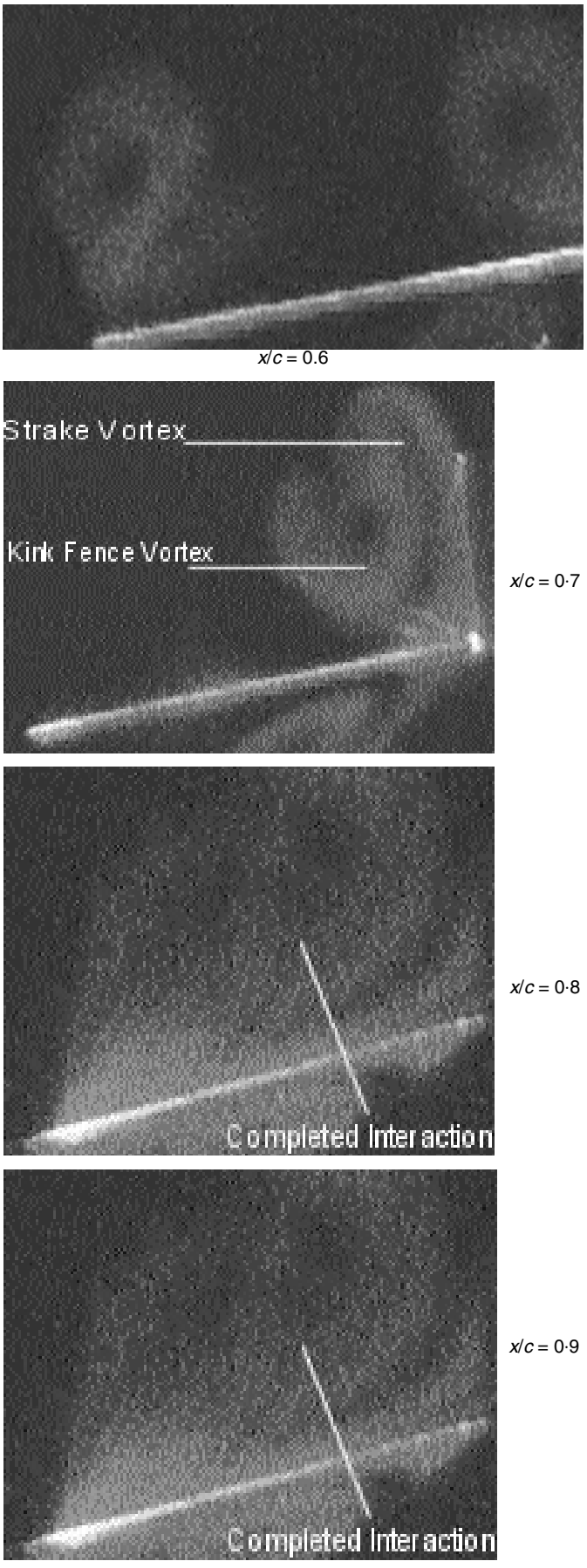


Figure 9. Spiralling interaction inboard of kink fence (α = 15°) (White arrow indicates direction of movement).

Figure 15 shows the results of using this method on a double-delta wing with apex fence. As seen from the figure, there is a characteristic dip at the vortex breakdown position when vortex half-width is plotted against the angle-of-attack. The breakdown is seen to occur at about 22·5° angle-of-attack and 0·8 chord. This is in excellent agreement with flow visualisation result. This feature was also evident when plain wing and kink fence data were plotted although it occurred at different chordwise positions.

Figure 16 shows the data presented in terms of chordwise positions with angle-of-attack as parameter. As seen from this figure, two distinct patterns are evident, depending on what interaction is dominant. The enveloping interaction displays a pattern of high initial half-width, followed by a steep fall, whilst the spiralling interaction shows a dip and then a rise in half-width, such that the curve is roughly symmetrical. The large differences seen in initial half-width are probably due to the effect of apex fences on the strake vortex changing as the angle-of-attack is increased. Secondly, the increase in half-width seen at 0·8 chord is possibly due to the instability of the coiling interaction, causing the vortex to expand earlier and further than when the enveloping interaction is occurring. While nothing more than qualitative judgement can be made based on these data, it is clear that vortex interaction pattern distinctly differs between low (≤20°) and high (≤20°) angles-of-attack as seen from these vortex half-width patterns.



x/*c* = 0.6

x/*c* = 0·7

x/*c* = 0·8

x/*c* = 0·9

Figure 10. Laser sheet smoke visualisation (α = 20°)

https://doi.org/10.1017/S0001924000004966 Published online by Cambridge University Press

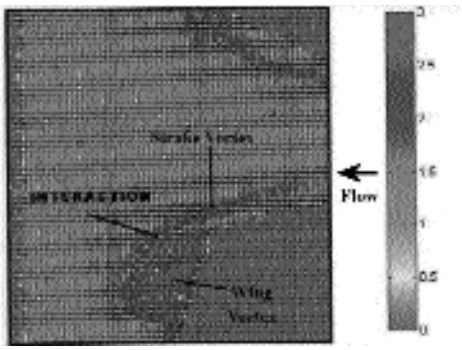


Figure 11. Interaction between the wing and strake vortices ($\alpha = 15°$).

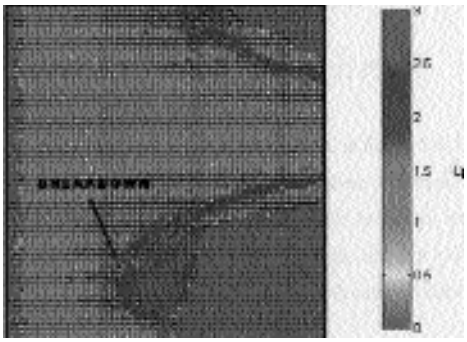


Figure 12. Pressure map showing vortex breakdown ($\alpha = 22{\cdot}5°$).

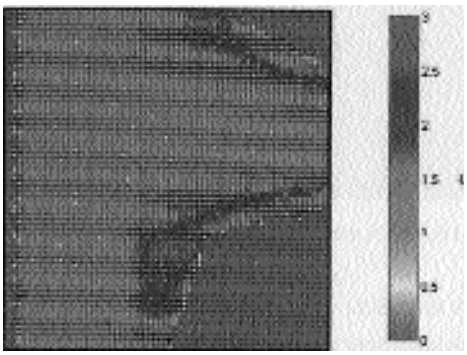


Figure 13. Pressure map showing loss of suction ($\alpha = 30°$).

8.0 REYNOLDS NUMBER EFFECTS

As noted in Section 2.2, both the wind tunnel and water tunnel models had sharp leading edges. It has been noted by Fisher *et al*[10]. that very good agreement on vortex breakdown data exists between wind tunnel, water tunnel and flight test experiments on F-18 double-delta model with leading edge extension (LEX). The Reynolds number variation in these tests ranged from $8{\cdot}3 \times 10^3$ to 13×10^6.

However, the present data showed that the type of interaction that occurs before breakdown is Reynolds number dependent. As the Reynolds number increased, outboard and downward movement of vortices occurred. This was accompanied by a change in interaction mechanism from that of spiralling to enveloping along with the forward movement of the vortex breakdown. These observations are also consistent with the results of Verhagen[11] and Hebbar[12].

9.0 SUMMARY AND CONCLUSIONS

The objective of this investigation was to look into the dynamics of vortex flow over a double-delta wing, including the effects of fences. Although the results revealed considerable information on the vortex behaviour of double-delta wings, substantial areas of uncertainty still remain.

Two interaction mechanisms were found to operate in the case of both plain and apex-fenced models. These were the enveloping and spiralling/coiling interactions. Each interaction had a different effect on the vortex flow. In the enveloping interaction, the wing vortex drew the strake vortex outboard and underneath itself. It occurred at lower angles-of-attack. In the spiralling/coiling interaction, the wing vortex was drawn inboard and around the strake vortex. This occurred at higher angles-of-attack. The change in mechanism appeared to occur when the strake vortex strength approached that of the wing vortex. The changeover occurred at $22{\cdot}5°$ angle-of-attack for the plain wing model and 20° angle-of-attack for the apex-fenced model. At low Reynolds numbers, the spiralling interaction was dominant, possibly due to the low strength of the wing vortex.

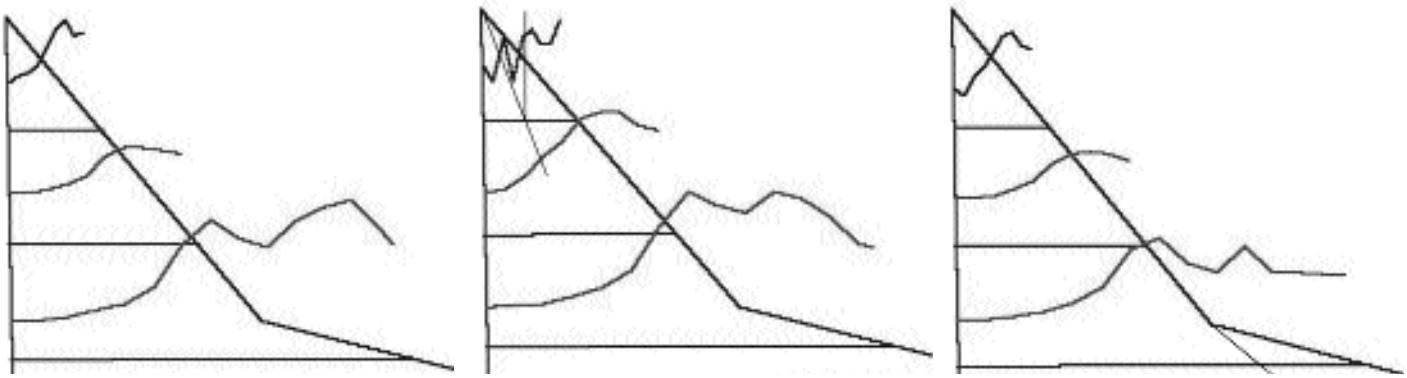
The apex fences strengthened the strake vortices but showed some initial instability. This was attributed to the merging of strake and apex fence vortices that hastened the changeover of interaction mechanism. Also, the breakdown position moved upstream somewhat. In contrast, the kink fences stabilised the vortex flow by introducing a vortex that interacted in a beneficial manner with the strake vortex. The severity of the vortex burst was also reduced.

As Reynolds number increased, an outboard and downward movement of vortices occurred. This was accompanied with a change of the dominant interaction mechanism from coiling to enveloping and upstream movement of vortex breakdown. These observations agree with the previous studies by Verhaagen, and Hebbar.

A correlation was found between vortex half-width and vortex breakdown position when the vortex half-width was plotted against angle-of-attack as per Greenwell and Wood. In addition, a correlation was also found between vortex half-width and interaction mechanism, when the half-width was plotted against chordwise position.

ACKNOWLEDGEMENTS

The authors would like to acknowledge the very considerable help of Jonathan Couldrick in the preparation of this paper.



(a)Plain wing (b) Apex fence (c) Kink fence

Figure 14. Planform overlay representations, ($\alpha = 20°$).

https://doi.org/10.1017/S0001924000004966 Published online by Cambridge University Press

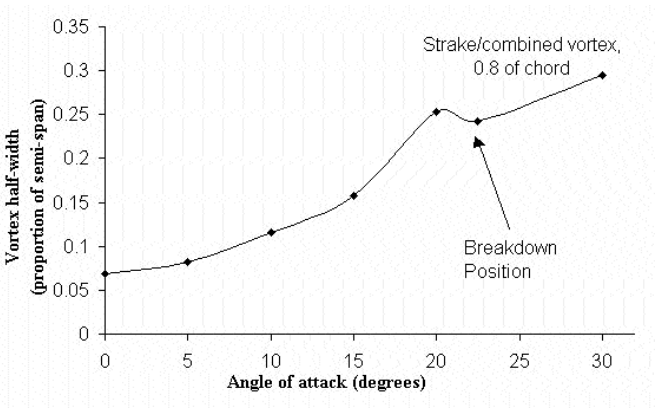


Figure 15. Vortex half-width against angle-of-attack model with apex fences.

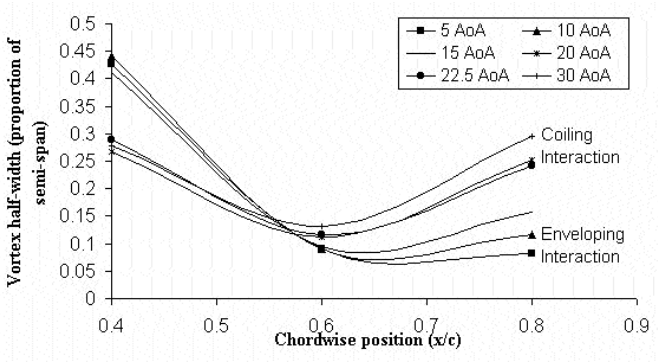


Figure 16. Vortex half-width against chordwise position, model fitted with apex fences strake/combined suction peak.

REFERENCES

1. VERHAAGEN, N.G., JENKINS, L.N., KERN, S.B. and WASHBURN, A.E. A study of the vortex flow over a 76°/40° double-delta wing, 1995, NASA, CR-195032.
2. HEBBAR, S.K., PLATZER, M.F. and ALKHOZAM, A.M. Experimental study of vortex flow control on double-delta wings using fillets, *J Aircr*, 1996, **33**, (4), pp 743-751.
3. EKATERINARIS, J.A., COUTLEY, R.L., SCHIFF, L.B. and PLATZER, M.F. Numerical investigation of high incidence flow over a double-delta wing, *J Aircr*, 1995, **32**, (3), pp 457-463.
4. KERN, S.B. Vortex flow control using fillets on a double-delta wing, *J Aircr*, 1993, **30**, (6), pp 818-825.
5. HOFFLER, K.D., RAO, D.M. and FRASSINELLI, M.C. Low-speed aerodynamics of apex fences on tailless delta configuration, *J Aircr*, 1988, **25**, (4), pp 295-301.
6. LAMAR, J.E. Analysis and design of strake-wing configurations, *J Aircr,* 1980, **17**, (1), pp 20-27.
7. WAHLS, R.A., VESS, R.J., and MOSKOVITZ, C.A. Experimental investigation of apex fence flaps on delta wings, *J Aircr*, 1996, **23**, (10), pp 789-797.
8. GREENWELL, D.I., and WOOD, N.J. Determination of vortex burst location on delta wings from surface pressure measurements, *AIAA J*, 1988, **30**, (11), pp 2736-2739.
9. KLEIN, C. Application of pressure sensitive paint (PSP) for determination of the instantaneous pressure field of models in a wind tunnel, Dissertation Gottingen, DZLR Report 97-55, 1997.
10. FISHER, D.F., COBLEIGH, B.R., BANKS, D.W., HALL, R.M. and WAHLS, R.W. Reynolds number effects at high angles-of-attack, NASA/TP-1998-206553, June 1999.
11. VERHAAGEN, N.G. Effects of Reynolds number on the flow over 76/40 - deg double-delta wings, AIAA 17th App Aero Dyn Conf, 1999, pp 142-152.
12. HEBBAR, S.K., PHATZER, M.F. and FRITZELAS, A.E. Reynolds number effects on the vortical flow structure generated by a double-delta wing, *Experiments in Fluids*, 2000, **28**, pp 206-216.

https://doi.org/10.1017/S0001924000004966 Published online by Cambridge University Press